Ocean Engineering 189 (2019) 106328

Contents lists available at ScienceDirect

Ocean Engineering

journal homepage: www.elsevier.com/locate/oceaneng

A six-DOF theoretical model for steady turning maneuver of a planing hull

Sasan Tavakoli [a], Abbas Dashtimanesh [b,c,*]

[a] Department of Infrastructure Engineering, The University of Melbourne, Melbourne, VIC, Australia
[b] Department of Engineering, Persian Gulf University, Bushehr, Iran
[c] Estonian Maritime Academy, Tallinn University of Technology, Tallinn, Estonia

ARTICLE INFO

Keywords:
Steady turning
Planing hull
Maneuver
2D+T theory

ABSTRACT

The current paper presents simulations for steady turning of a planing craft by developing a new mathematical model. To solve the problem, it is assumed that the craft is free in six-degrees of freedom and all motions are strongly coupled. Maneuvering forces and moments acting on the vessel are computed using 2D + T theory. Virtual added mass terms of two-dimensional (2D) sections are integrated over the entire length of the craft. The final equation for the motion of the vessel in six-degrees of freedom is obtained which is then solved in the time domain. Final three-dimensional (3D) forces and moments contain strongly coupled added mass, damping, steady maneuvering, and restoring hydrostatic forces and moments. Simulations are compared against experimental data and it is shown that the developed method has reasonable accuracy in prediction of turning motion of two planing vessels. Effects of beam Froude Number and rudder angle on steady turning motion of a planing hull have also been studied. It is found that when the vessel is free in six-degrees of freedom, the turning radius and yaw rate of the vessel are smaller while the steady surge speed is not affected significantly.

1. Introduction

Prediction of the steady turning motion of planing hulls, although an important aspect, has received scant regard in the hydrodynamic design of the high-speed craft. Nonlinear behavior of the vessel as well as coupled heave, pitch, and roll motions, which can generate forces and moments in the horizontal plane tend to complicate the problem (see e. g. Tavakoli et al., 2017b). Traditional mathematical models used for maneuvering simulation of ships are not suitable for simulation of maneuvering motion of planing hulls (see discussions of Morabito et al., 2014 and Conclusion of Morabito, 2015). Recent advances in mathematical modeling (based on the 2D + T theory) of heeled/yawed planing hulls can be further developed for maneuvering simulation of these vessels (see e. g. Tavakoli et al., 2018a). Specifically, two different mathematical models have developed by authors for mathematical simulations of steady drift test (Dashtimanesh et al. 2019a) and planar motion mechanism (PMM) test of planing hulls (Tavakoli and Dashtimanesh, 2018). Both mathematical models showed good ability to compute maneuvering forces/moments acting on a planing hull (note that authors performed a wide range of comparison against experimental data of Brown and Klosinski (1994a, b), Katayama et al. (2006) and Tajima et al. (1999) in their recent publications). At the current stage, previous progress in mathematical modelling of planing hulls motion can be followed, as we will show, to develop a mathematical model for simulation of six-degrees of freedom (6DOF) of planing hulls in turning. In the current paper, a mathematical model is established using 2D + T theory to simulate the turning motion of planing hulls in 6DOF.

Early studies in the context of planing hulls maneuvering were performed by Smiley (1952) and Savitsky (1958), who respectively explored hydrodynamic forces acting on yawed and heeled planing hulls. Later, the majority of the researchers such as Sugai (1964) as well as Blount and Codega (1992) investigated the instabilities of planing hulls in the horizontal plane. Meanwhile, Denny (1991) proposed a maneuvering simulation for planing hulls by neglecting the effects of heave, pitch, and roll motions. Lewandowski (1994, 1995) presented a mathematical model for prediction of the trajectory of a planing hull in the horizontal plane. His method was extremely helpful in gaining insight into the turning motion of planing hulls and their stability in the horizontal plane. But, his method relies on empirical equations and is unable to consider six-degrees of freedom for a wide range of planing hulls (see discussion in Morabito, 2015). Toxopeus (1996a) developed a mathematical model for prediction of the 6DOF motion of planing hulls. His method was able to simulate the motion of the vessel. But, for many cases (especially for the case of added mass forces), traditional equations

* Corresponding author. Department of Engineering, Persian Gulf University, Bushehr, Iran.
E-mail address: a.dashtimanesh@pgu.ac.ir (A. Dashtimanesh).

https://doi.org/10.1016/j.oceaneng.2019.106328
Received 28 January 2019; Received in revised form 11 July 2019; Accepted 15 August 2019
Available online 5 September 2019

Nomenclature

$a^{'}$	Non-dimensional parameter used for transom reduction function
A_T	Transom area (m^2)
b_1, b_2	Half beam of starboard and port (m)
B	Beam (m)
c	Half-wetted beam of the section (m)
$\dot{c}$	Time rate of half-wetted beam of the section (m/s)
c_1, c_2	Half-wetted beam of the starboard and port (m)
$\dot{c_1}$, $\dot{c_2}$	Time rate of half-wetted beam of the starboard and port (m/s)
C_f	Frictional resistance coefficient
C_{DT}	Transom suction drag coefficient
f_B	2D hydrostatic force (N/m)
$Fn_B = u/\sqrt{gB}$	Beam Froude Number
g	Gravity acceleration
$Gxyz$	Body fixed frame (Coordinate system)
I_{ij}	Second moment of 2D sectional added mass in direction of i due to motion in direction of j (kg-m^2)
I_{xx}, I_{yy}, I_{zz}	Mass moment of inertia in x, y and z directions (kg -m^2)
K^{2D}	2D angular moment (N-m/m)
K_p, K_q, K_r	Damping moments due to angular motions (roll, pitch and yaw) in roll direction (N-m)
$K_{\dot{p}}$, $K_{\dot{q}}$, $K_{\dot{r}}$	Added mass moments due to angular motions (roll, pitch and yaw) in roll direction (N-m)
K_u, K_v, K_w	Damping moments due to linear motions (surge, sway and heave) in roll direction (N-m)
$K_{\dot{u}}$, $K_{\dot{v}}$, $K_{\dot{w}}$	Added mass moments due to linear motions (surge, sway and heave) in roll direction (N)
K_z, K_φ, K_θ	Hydrostatic restoring moment in heave direction due to heave, roll and pitch motions (N-m)
K, M, N	Maneuvering moments in roll, pitch and yaw directions (N)
K^*, M^*, N^*	Maneuvering forces in roll, pitch and yaw directions excluding added mass forces (N-m)
K^{ST}, M^{ST}, N^{ST}	Maneuvering steady moments in roll, pitch and yaw directions (N-m)
m	Mass of the boat (kg)
m_B	2D hydrostatic moment (N-m/m)
m_{ij}	2D added mass in direction of i due to motion in direction of j (kg/m or kg -m^2/m)
M_{ij}	Integration of 2D sectional added mass in direction of i due to motion in direction of j (kg)
M_p, M_q, M_r	Damping moments due to angular motions (roll, pitch and yaw) in pitch direction (N-m)
$M_{\dot{p}}$, $M_{\dot{q}}$, $M_{\dot{r}}$	Added mass moments due to angular motions (roll, pitch and yaw) in pitch direction (N-m)
M_u, M_v, M_w	Damping moments due to linear motions (surge, sway and heave) in pitch direction (N-m)
$M_{\dot{u}}$, $M_{\dot{v}}$, $M_{\dot{w}}$	Added mass moments due to linear motions (surge, sway and heave) in pitch direction (N)
N_p, N_q, N_r	Damping moments due to angular motions (roll, pitch and yaw) in yaw direction (N-m)
$N_{\dot{p}}$, $N_{\dot{q}}$, $N_{\dot{r}}$	Added mass moments due to angular motions (roll, pitch and yaw) in yaw direction (N-m)
N_u, N_v, N_w	Damping moments due to linear motions (surge, sway and heave) in yaw direction (N-m)
$N_{\dot{u}}$, $N_{\dot{v}}$, $N_{\dot{w}}$	Added mass moments due to linear motions (surge, sway and heave) in yaw direction (N)
N_z, N_φ, N_θ	Hydrostatic restoring moment in heave direction due to heave, roll and pitch motions (N-m)
$Ox_e y_e z_e$	Earth frame (Coordinate system)
$O'x_h y_h z_h$	Hydrodynamic frame (Coordinate system)
p, $\dot{p}$	Roll speed (rad/s) and acceleration (rad/s^2)
q, $\dot{q}$	Pitch speed (rad/s) and acceleration (rad/s^2)
Q_{ij}	First moment of 2D sectional added mass in direction of i due to motion in direction of j (kg -m)
R	Transom reduction function (−)
r, $\dot{r}$	Yaw speed (rad/s) and acceleration (rad/s^2)
S	Wetted surface of the vessel (m^2)
T	Thrust force (N)
t	Time (s)
u, $\dot{u}$	Surge speed (m/s) and acceleration (m/s^2)
v, $\dot{v}$	Sway speed (m/s) and acceleration (m/s^2)
w, $\dot{w}$	Heave speed (m/s) and acceleration (m/s^2)
W	Weight of the vessel (N)
x_{CG}	Longitudinal position of CG with respect to transom (m)
x_T	Longitudinal Position of transom with in body frame (m)
x_δ	Thrust force distance from CG (m)
X_e	Transitional velocities in earth frame
X_p, X_q, X_r	Damping forces due to angular motions (roll, pitch and yaw) in surge direction (N)
$X_{\dot{p}}$, $X_{\dot{q}}$, $X_{\dot{r}}$	Added mass forces due to angular motions (roll, pitch and yaw) in surge directionN
X_u, X_v, X_w	Damping forces due to linear motions (surge, sway and heave) in surge direction (N)
$X_{\dot{u}}$, $X_{\dot{v}}$, $X_{\dot{w}}$	Added mass forces due to linear motions (surge, sway and heave) in surge direction (N)
X, Y, Z	Maneuvering forces in surge, sway and heave directions (N)
X^*, Y^*, Z^*	Maneuvering forces in surge, sway and heave directions excluding added mass forces (N)
X^{ST}, Y^{ST}, Z^{ST}	Maneuvering steady forces in surge, sway and heave directions (N)
Y^{2D}	2D horizontal force (N/m)
Y_p, Y_q, Y_r	Damping forces due to angular motions (roll, pitch and yaw) in sway direction (N)
$Y_{\dot{p}}$, $Y_{\dot{q}}$, $Y_{\dot{r}}$	Added mass forces due to angular motions (roll, pitch and yaw) in sway direction (N)
Y_u, Y_v, Y_w	Damping forces due to linear motions (surge, sway and heave) in sway direction (N)
$Y_{\dot{u}}$, $Y_{\dot{v}}$, $Y_{\dot{w}}$	Added mass forces due to linear motions (surge, sway and heave) in sway direction (N)
z_{CG}	Vertical position of CG with respect to transom (m)
Z^{2D}	2D vertical force (N/m)
Z_p, Z_q, Z_r	Damping due to angular forces (roll, pitch and yaw) in heave direction (N)
$Z_{\dot{p}}$, $Z_{\dot{q}}$, $Z_{\dot{r}}$	Added mass forces due to angular forces (roll, pitch and yaw) in heave direction (N)
Z_u, Z_v, Z_w	Damping forces due to linear motions (surge, sway and heave) in heave direction (N)
$Z_{\dot{u}}$, $Z_{\dot{v}}$, $Z_{\dot{w}}$	Added mass forces due to linear motions (surge, sway and heave) in heave direction (N)
Z_z, Z_φ, Z_θ	Hydrostatic restoring force in heave direction due to heave, roll and pitch motions (N)
β	Deadrise angle of the vessel (Deg.)
β_1, β_2	Deadrise angle of starboard and port (Deg.)
δ	Thrust force angle (Deg.)
$\boldsymbol{\eta}$, $\dot{\boldsymbol{\eta}}$	Unknown vector (m/s for linear motion and rad/s for angular motion) and its time rate (m/s^2 for linear motion and rad/s^2 for angular motion)
θ	Pitch angle (rad)
ξ, $\dot{\xi}$, $\ddot{\xi}$	Vertical displacement (m), speed (m/s) and acceleration (m/s^2) of the 2D wedge entering water
μ	Asymmetric parameter (m)
$\dot{\mu}$	Time rate of asymmetric parameter (m)
ρ	Water density (kg -m^3)
ϕ_i	Velocity potential due to motion in direction i

φ	Roll angle (rad)	ψ	Yaw angle (rad)
$\chi, \dot{\chi}, \ddot{\chi}$	Horizontal displacement (m), speed (m/s) and acceleration (m/s^2) of the 2D wedge entering water	$\mathbf{\Omega}_e$	Angular velocities in earth frame

developed for displacement ships were utilized, which are not accurate for the case of planing hulls (Dashtimanesh et al., 2017). Furthermore, he presented specific equations for the computation of maneuvering forces of a series of planing hulls (Toxopeus, 1996b).

In addition to the mentioned research, Katayama et al. (2005) conducted steady drift tests on planing hulls, commenting that during the turning motion of planing hulls heave and pitch motions vary in time, affecting the hydrodynamic maneuvering forces and moments. Katayama et al., (2006) performed experimental tests and mathematical simulations (by considering the effects of heave and pitch motion of forces and moments) of the turning motion of a prismatic planing hull. It was found that when heave and pitch motions are considered (i.e. heave and pitch motions are set to be free), the accuracy of mathematical simulations increases. To simulate the turning motion of planing hulls more accurately, Katayama et al. (2009) used a large range of steady test data and interpolated hydrodynamic coefficients of the vessel using its instantaneous heave and pitch. Their method can work well, however, the availability of steady test data is a prerequisite, which cannot be easily accessed, i. e., we need all drift test data (of a vessel we want to model) to use that mathematical model. Also, Morabito et al. (2014), as well as Bhawsinka (2008) have discussed about the importance of considering heave and pitch motions on forces/moments in the maneuvering motion.

The other option to simulate maneuvering motion of planing hulls is to use the 2D + T theory. This method utilizes the solution of water entry of a solid wedge section, which is similar to the section of a planing craft (Sun and Faltinsen, 2007). In recent years, this method has shown good ability in hydrodynamic modeling of planing hulls (Ghadimi et al., 2017a; Tavakoli et al., 2017b). The key to its success lies in the possibility to provide a pattern for coupling motions in vertical, horizontal and transverse planes, which in turn, allows the simulation of 6DOF motion of vessel (see the work of Xu et al., 1999 and Judge et al., 2004; where they have discussed this idea). The other advantage of this method is that rapid simulations can be undertaken (see e. g. Zarnick, 1978 as well as Garme and Rosen, 2003). Recently, Morabito (2015) as well as Tavakoli and Dashtimanesh (2017) have shown that this method provides accurate results for the drift test of a planing hull. In addition, by combining previous asymmetric 2D + T models (see Tavakoli et al., 2015; Ghadimi et al., 2016a), Dashtimanesh et al., 2019a, as well as Tavakoli and Dashtimanesh (2018) presented oblique-asymmetric simulations for steady asymmetric drift and PMM tests of planing hulls, as mentioned earlier (in the first paragraph of the current section). In the current paper, an attempt has been made to extend 2D + T theory for modeling of planing hulls turning maneuver in 6DOF, to provide understanding about the turning motion of these vessels.

In the present paper, a mathematical model for simulation of the steady turning motion of a planing craft has been developed by using 2D + T theory and solution of water entry of a wedge section into water. Mathematical formulations for the prediction of hydrodynamic forces and moments acting on the body are presented in section 2. These formulations are developed by extending 2D (vertical) forces and (angular) moments over the wetted length of the vessel. 3D Forces and moments all have nonlinear nature and effects of vertical motion on horizontal forces/moments are implemented. The guideline for simulation of the problem has been explained in section 3. The results of the simulation have been presented in section 4. Comparative analysis against previous experimental data is presented and it is shown that the current 6DOF simulation can predict the turning motion of two different prismatic planing hulls accurately. Turning motion of a planing vessel in different situations is simulated and it is shown how the changes in Froude

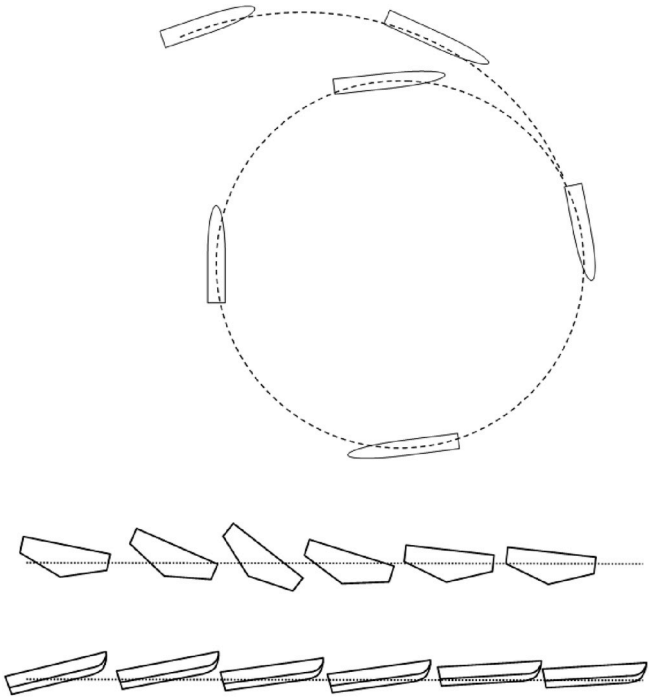

Fig. 1. A planing hull turning into starboard: the trajectory of the vessel in the horizontal plane (up), the roll motion (middle) and vertical motions (low) during the turning.

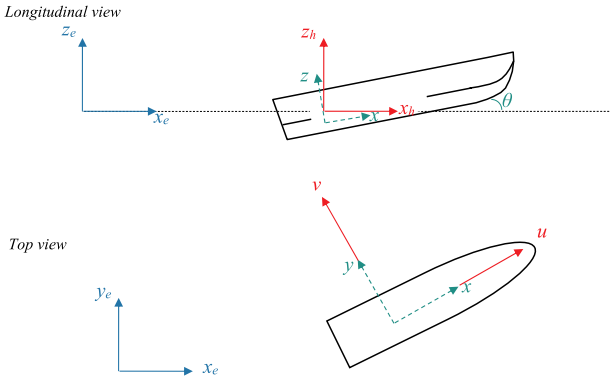

Fig. 2. Coordinate systems considered for the current problem (steady turning of a planing hull).

Number and thrust angle can affect the turning motion of a planing boat. The effects of the degrees of freedom on the turning motion of the vessel are also investigated. Concluding remarks and future work have been included in section 5.

2. Mathematical model

2.1. Problem definition

A hard-chine planing vessel with a beam of B, deadrise angle of β, is assumed to advance in the planing regime, while it turns into port/starboard (see Fig. 1). As the craft undergoes unsteady turning, all motions are coupled and therefore, changes in running attitudes (see

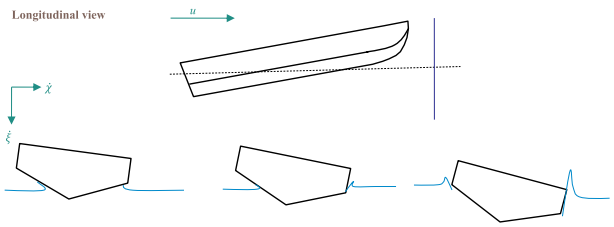

Fig. 3. 2D + T theory for solving turning motion of a planing craft.

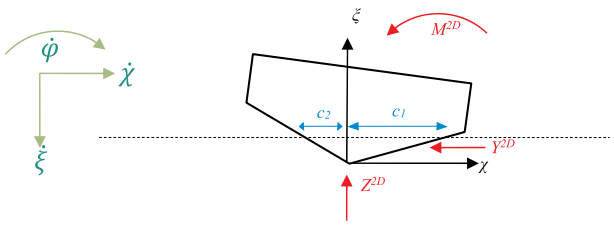

Fig. 4. A 2D wedge body entering water with oblique and rotational velocities (Javanmardi et al., 2018).

Katayama et al., 2005, 2006; Tavakoli et al., 2018), roll motion (see Bowles and Blount, 2012), and speed reduction occur. It is expected that the craft finally reaches steady state condition (see Kim and Kim, 2017).

The governing equation on the motion of the vessel is formulated using three right-handed coordinate systems (see examples of the coordinates systems in the research of Subramanian and Beck, 2015) as shown in Fig. 2. The first one is an earth-fixed coordinate system, shown by $Ox_e y_e z_e$. The second coordinate system is a hydrodynamic coordinate system, denoted with $O'x_h y_h z_h$, which moves with the vessel. This coordinate system has only transitional and rotational speeds of the vessel and has no vertical motion. The final coordinate system considered in the current study is a body-fixed coordinate system, $Gxyz$, which is placed at the center of gravity (CG). The governing equation on the motion of the vessel can be written as:

$$\begin{aligned} &m\dot{u} + m(qw - vr) = X + T\cos\delta \\ &m\dot{v} + m(ur - pw) = Y + T\sin\delta \\ &m\dot{w} + m(pv - qu) = Z + W \\ &I_{xx}\dot{p} - (I_{yy} - I_{zz})qr = K \\ &I_{yy}\dot{q} - (I_{zz} - I_{xx})pr = M \\ &I_{zz}\dot{r} - (I_{xx} - I_{yy})pq = N + x_\delta(T\sin\delta) \end{aligned} \tag{1}$$

where m is the mass of the vessel, I_{ii} is the mass moment of inertia in direction of i (further information about the inertia of planing boats can be found in the work of Toxopeus, 1996a). u, v and w are surge, sway and heave velocities, respectively. p, q and r are the rotational velocities in roll, pitch and yaw directions, respectively. X, Y and Z respectively show the surge, sway and heave forces. K, M and N denote roll, pitch and yaw moments. T refers to the thrust force and δ stands for the inclination angle of thrust force. x_δ is the distance between the thrust force and CG. W is the weight force of the vessel.

2.2. 2D + T theory

It is assumed that the vessel travels through a transverse plane, as displayed in Fig. 3 (Further information can be found in Tavakoli et al., 2018c and Niazmand Bilandi 2019). The problem is simplified to the water entry of a wedge section with oblique and rotational speeds. Vertical and oblique velocities of the section are computed by

$$\dot{\xi} = u\sin\theta + w\cos\theta - x\dot{\theta}, \tag{2}$$

$$\dot{\chi} = u\sin\psi + v\cos\psi - x\dot{\psi} \tag{3}$$

Using the momentum variation (see von Karman, 1929), 2D (vertical and horizontal) forces and the (angular) moment (see Fig. 4) acting on the section are computed as

$$Y^{2D} = -\left((m_{\chi\chi}\ddot{\chi}) + (\dot{m}_{\chi\chi}\dot{\chi}) + (m_{\chi\xi}\ddot{\xi}) + (\dot{m}_{\chi\xi}\dot{\xi}) + (m_{\chi\phi}\ddot{\varphi}) + (\dot{m}_{\chi\phi}\dot{\varphi})\right) \tag{4}$$

$$Z^{2D} = -\left((m_{\xi\chi}\ddot{\chi}) + (\dot{m}_{\xi\chi}\dot{\chi}) + (m_{\xi\xi}\ddot{\xi}) + (\dot{m}_{\xi\xi}\dot{\xi}) + (m_{\xi\phi}\ddot{\varphi}) + (\dot{m}_{\xi\phi}\dot{\varphi})\right) \tag{5}$$

$$M^{2D} = -\left((m_{\varphi\chi}\ddot{\chi}) + (\dot{m}_{\varphi\chi}\dot{\chi}) + (m_{\varphi\xi}\ddot{\xi}) + (\dot{m}_{\varphi\xi}\dot{\xi}) + (m_{\varphi\varphi}\ddot{\varphi}) + (\dot{m}_{\varphi\varphi}\dot{\varphi})\right) \tag{6}$$

where m_{ij} is the 2D added mass in the direction of i due to motion in the direction of j (see Tavakoli et al., 2018). The term that is a product of the time rate of the added mass and the velocity shows the 2D damping force (see Faltinsen et al., 1977; Payne, 1995; Ghadimi et al., 2017b).

Added mass terms are computed as

$$m_{ij} = \rho\int_S \phi_j n_i dS \tag{7}$$

where ϕ_j is the potential due to motion in j direction and n_i is the normal unit vector (see Tavakoli et al., 2017a) in i direction (Newman, 1977). Using previous findings of Dashtimanesh et al. 2019a and Ghadimi et al. 2017c, added mass terms can be computed (see equations in Dashtimanesh et al., 2019).

To compute added mass terms, $\beta_1 = \beta$-φ (instantaneous deadrise angle of the starboard) and $\beta_2 = \beta$+φ (instantaneous deadrise angle of the port) are needed. Besides, c and μ, which are half-wetted beam and asymmetric parameters (see Korobkin and Malenica, 2005 as well as Qin et al., 2011) should be computed. The method for computation of half-wetted beam and asymmetric parameter is presented in Appendix A. The 2D hydrostatic force (f_B) is computed by

$$f_B = \rho g\left(\frac{c_1 d}{2} + \frac{c_2 d}{2}\right) \tag{8}$$

where, d is water draft at section. Note that 2D hydrostatic force is computed by considering the (Wagner) water pile-up (Tavakoli, 2018a). The 2D angular moment (m_B) caused by hydrostatic pressure is computed by

$$m_B = \rho g\left(\frac{c_1 d}{2}\frac{c_1}{3} - \frac{c_2 d}{2}\frac{c_2}{3}\right) \tag{9}$$

Note that, c_i is the half-wetted beam of side i (i = 1 and 2 respectively refer to starboard and port) is computed by consideration of water pile-up (see Appendix A).

Three dimensional (3D) forces and moments are computed by extending sectional forces and moments over the entire length of the vessel (see Martin, 1976). 3D forces are computed by

$$X = \left(\int_L R(x)Z^{2D}(x)dx\right)\sin\theta + \left(\int_L R(x)Y^{2D}(x)dx\right)\sin\psi + \frac{1}{2}\rho u^2 S(C_f + \Delta C_f) + \frac{1}{2}\rho u^2 C_{DT}A_T, \tag{10}$$

$$Y = \left(\int_L R(x)Y^{2D}(x)dx\right)\cos\psi, \tag{11}$$

$$Z = \left(\int_L R(x)Z^{2D}(x)dx\right)\cos\theta + \left(\int_L R(x)f_B(x)dx\right). \tag{12}$$

3D moments acting on the vessel are determined by

$$K = \left(\int_L R(x)M^{2D}(x)dx\right) + \left(\int_L R(x)\mathrm{m}_B(x)dx\right), \tag{13}$$

$$M = -\left(\left(\int_L R(x)xZ^{2D}(x)dx\right) + \left(\int_L R(x)xf_B(x)dx\right)\right), \tag{14}$$

$$N = -\left(\int_L R(x)xY^{2D}(x)dx\right) \tag{15}$$

In the above equations $R(x)$ is the reduction function, which is used to apply effects of transom on the hydrodynamic and hydrostatic pressure, i. e. reduction function (which is an empirical equation) affects the hydrostatic and hydrodynamic pressure by making the sectional forces to be zero at transom (see Morabito, 2014; Ghadimi et al., 2019). Here, the transom reduction function introduced by Garme's (2005) is used as

$$R(x) = \tan h\left(\frac{2.5}{a`BFn_B}(x - x_T)\right) \tag{16}$$

where Fn_B is the beam Froude Number of the vessel and x_T refers to transom position with respect to CG. Moreover, a' is a constant empirical coefficient that equals 0.35 (see Garme, 2005; Tavakoli et al., 2018a).

The last terms of equation (10) refer to the forces caused by the friction (corresponds to $\frac{1}{2}\rho u^2 S(C_f + \Delta C_f)$) and transom suction (corresponds to $\frac{1}{2}\rho u^2 C_{DT} A_T$). C_f is the frictional drag coefficient obtained by using ITTC '57 formulation (Savitsky, 1964). S is the wetted surface and is computed (see Ghadimi et al., 2014) by

$$S = \int_L \left(\frac{c_1}{sin\beta_1} + \frac{c_2}{sin\beta_2}\right)dx \tag{17}$$

C_{DT} is the transom suction drag coefficient, introduced by Payne (1988). The force caused by transom suction refers to the drag force appearing when the transom is dry (see page 45 of Payne, 1988 and also check Dashtimanesh et al., 2019b). Payne (1995) proposed to consider a value ranging between 0.08 and 0.22 for C_{DT}(here we assumed the mean value). A_T is the transom area. The integrals of forces and moments are found as

where

$$\int_L R(x)Y^{2D}(x)dx = \begin{pmatrix} -M_{\dot{\chi}\xi}sin\theta\dot{u} - M_{\dot{\chi}\xi}cos\theta\dot{w} + Q_{\dot{\chi}\xi}\dot{q} + M_{\dot{\chi}\xi}q(w\sin\theta - u\cos\theta) \\ -M_{\dot{\chi}\chi}\sin\psi\dot{u} - M_{\dot{\chi}\chi}\cos\psi\dot{w} + Q_{\dot{\chi}\chi}\dot{r} + M_{\dot{\chi}\chi}r(v\sin\psi - u\cos\psi) \\ -M_{\dot{\chi}\varphi}\dot{p} - u\dot{\xi}m_{\dot{\chi}\xi}|_{x=x_T} - \int_L R(x)\dot{\xi}\dot{m}_{\dot{\chi}\xi}dx - u\dot{\chi}m_{\dot{\chi}\chi}|_{x=x_T} \\ -\int_L R(x)\dot{\chi}\dot{m}_{\dot{\chi}\chi}dx - u\dot{\varphi}m_{\dot{\chi}\varphi}|_{x=x_T} - \int_L R(x)\dot{\varphi}\dot{m}_{\dot{\chi}\varphi}dx \end{pmatrix} \tag{18}$$

$$\int_L R(x)Z^{2D}(x)dx = \begin{pmatrix} -M_{\dot{\xi}\xi}sin\theta\dot{u} - M_{\dot{\xi}\xi}cos\theta\dot{w} + Q_{\dot{\xi}\xi}\dot{q} + M_{\dot{\xi}\xi}q(w\sin\theta - u\cos\theta) \\ -M_{\dot{\xi}\chi}\sin\psi\dot{u} - M_{\dot{\xi}\chi}\cos\psi\dot{w} + Q_{\dot{\xi}\chi}\dot{r} + M_{\dot{\xi}\chi}r(v\sin\psi - u\cos\psi) \\ -M_{\dot{\xi}\varphi}\dot{p} - u\dot{\xi}m_{\dot{\xi}\xi}|_{x=x_T} - \int_L R(x)\dot{\xi}\dot{m}_{\dot{\xi}\xi}dx - u\dot{\chi}m_{\dot{\xi}\chi}|_{x=x_T} \\ -\int_L R(x)\dot{\chi}\dot{m}_{\dot{\xi}\chi}dx - u\dot{\varphi}m_{\dot{\xi}\varphi}|_{x=x_T} - \int_L R(x)\dot{\varphi}\dot{m}_{\dot{\xi}\varphi}dx \end{pmatrix} \tag{19}$$

$$\int_L R(x)M^{2D}(x)dx = \begin{pmatrix} -M_{\dot{\varphi}\xi}sin\theta\dot{u} - M_{\dot{\varphi}\xi}cos\theta\dot{w} + Q_{\dot{\varphi}\xi}\dot{q} + M_{\dot{\varphi}\xi}q(w\sin\theta - u\cos\theta) \\ -M_{\dot{\varphi}\chi}\sin\psi\dot{u} - M_{\dot{\varphi}\chi}\cos\psi\dot{w} + Q_{\dot{\varphi}\chi}\dot{r} + M_{\dot{\varphi}\chi}r(v\sin\psi - u\cos\psi) \\ -M_{\dot{\varphi}\varphi}\dot{p} - u\dot{\xi}m_{\dot{\varphi}\xi}|_{x=x_T} - \int_L R(x)\dot{\xi}\dot{m}_{\dot{\varphi}\xi}dx - u\dot{\chi}m_{\dot{\varphi}\chi}|_{x=x_T} \\ -\int_L R(x)\dot{\chi}\dot{m}_{\dot{\varphi}\chi}dx - u\dot{\varphi}m_{\dot{\varphi}\varphi}|_{x=x_T} - \int_L R(x)\dot{\varphi}\dot{m}_{\dot{\varphi}\varphi}dx \end{pmatrix} \tag{20}$$

$$\int_L R(x)Z^{2D}(x)xdx = \begin{pmatrix} -Q_{\dot{\xi}\xi}sin\theta\dot{u} - Q_{\dot{\xi}\xi}cos\theta\dot{w} + I_{\dot{\xi}\xi}\dot{q} + Q_{\dot{\xi}\xi}q(w\sin\theta - u\cos\theta) \\ -Q_{\dot{\xi}\chi}\sin\psi\dot{u} - Q_{\dot{\xi}\chi}\cos\psi\dot{w} + I_{\dot{\xi}\chi}\dot{r} + Q_{\dot{\xi}\chi}r(v\sin\psi - u\cos\psi) \\ -Q_{\dot{\xi}\varphi}\dot{p} - ux\dot{\xi}m_{\dot{\xi}\xi}|_{x=x_T} - \int_L R(x)\dot{\xi}\dot{m}_{\dot{\xi}\xi}xdx - ux\dot{\chi}m_{\dot{\xi}\chi}|_{x=x_T} \\ -\int_L R(x)\dot{\chi}\dot{m}_{\dot{\xi}\chi}xdx - ux\dot{\varphi}m_{\dot{\xi}\varphi}|_{x=x_T} - \int_L R(x)\dot{\varphi}\dot{m}_{\dot{\xi}\varphi}xdx \end{pmatrix} \tag{21}$$

$$\int_L R(x)Y^{2D}(x)xdx = \begin{pmatrix} -Q_{\dot{\chi}\xi}sin\theta\dot{u} - Q_{\dot{\chi}\xi}cos\theta\dot{w} + I_{\dot{\chi}\xi}\dot{q} + Q_{\dot{\chi}\xi}q(w\sin\theta - u\cos\theta) \\ -Q_{\dot{\chi}\chi}\sin\psi\dot{u} - Q_{\dot{\chi}\chi}\cos\psi\dot{w} + I_{\dot{\chi}\chi}\dot{r} + Q_{\dot{\chi}\chi}r(v\sin\psi - u\cos\psi) \\ -Q_{\dot{\chi}\varphi}\dot{p} - ux\dot{\xi}m_{\dot{\chi}\xi}|_{x=x_T} - \int_L R(x)\dot{\xi}\dot{m}_{\dot{\chi}\xi}xdx - ux\dot{\chi}m_{\dot{\chi}\chi}|_{x=x_T} \\ -\int_L R(x)\dot{\chi}\dot{m}_{\dot{\chi}\chi}xdx - ux\dot{\varphi}m_{\dot{\chi}\varphi}|_{x=x_T} - \int_L R(x)\dot{\varphi}\dot{m}_{\dot{\chi}\varphi}xdx \end{pmatrix} \tag{22}$$

Table 1
Principal characteristics of the investigated planing hulls.

Parameter	Value of parameter	
	Katayama et al. (2006)	Kim and Kim (2017)
Length of overall (m)	0.936	3.407
Beam (m)	0.18	0.937
Mass (kg)	3.08	231
β (degrees)	15.25	16 at transom and 24 at midship

$$M_{ij} = \int_L R(x) m_{ij} dx \tag{23}$$

$$Q_{ij} = \int_L R(x) x m_{ij} dx$$

$$I_{ij} = \int_L R(x) x^2 m_{ij} dx \qquad i,j = \chi, \xi, \varphi$$

Substituting forces and moments (Eqs. (19)–(24)) in the governing equation (Eq. (1)), the final motion equation of a planing hull in turning is obtained as

$$\begin{aligned}
&(m - X_{\dot u})\dot u - X_{\dot v}\dot v - X_{\dot w}\dot w - X_{\dot p}\dot p - X_{\dot q}\dot q - X_{\dot r}\dot r + m(qw - vr) = X^* + T\cos\delta - Y_{\dot u}\dot u + (m - Y_{\dot v})\dot v - Y_{\dot w}\dot w - Y_{\dot p}\dot p - Y_{\dot q}\dot q - Y_{\dot r}\dot r + m(ur - pw) = Y^* + T\sin\delta \\
&-Z_{\dot u}\dot u - Z_{\dot v}\dot v + (m - Z_{\dot w})\dot w - Z_{\dot p}\dot p - Z_{\dot q}\dot q - Z_{\dot r}\dot r + m(pv - qu) = Z^* + W - K_{\dot u}\dot u - K_{\dot v}\dot v - K_{\dot w}\dot w + (I_{xx} - K_{\dot p})\dot p - K_{\dot q}\dot q - K_{\dot r}\dot r - (I_{yy} - I_{zz})qr = K^* \\
&-M_{\dot u}\dot u - M_{\dot v}\dot v - M_{\dot w}\dot w - M_{\dot p}\dot p + (I_{yy} - M_{\dot q})\dot q - M_{\dot r}\dot r - (I_{xx} - I_{zz})pr = M^* - N_{\dot u}\dot u - N_{\dot v}\dot v - N_{\dot w}\dot w - N_{\dot p}\dot p - N_{\dot q}\dot q + (I_{zz} - N_{\dot r})\dot r - (I_{xx} - I_{yy})pq = N^* + x_\delta(T\sin\delta). \\
&-N_{\dot u}\dot u - N_{\dot v}\dot v - N_{\dot w}\dot w - N_{\dot p}\dot p - N_{\dot q}\dot q + (I_{zz} - N_{\dot r})\dot r - (I_{xx} - I_{yy})pq = N^* + x_\delta(T\sin\delta). \\
&-N_{\dot u}\dot u - N_{\dot v}\dot v - N_{\dot w}\dot w - N_{\dot p}\dot p - N_{\dot q}\dot q + (I_{zz} - N_{\dot r})\dot r - (I_{xx} - I_{yy})pq = N^* + x_\delta(T\sin\delta).
\end{aligned} \tag{24}$$

where any parameter with a * superscript refers to forces (for the case of X, Y and Z) and moments (for the case of K, M and N) excluding added mass contribution, i. e. any force or moment with * shows contribution of damping, steady maneuvering forces and hydrostatic restoring forces and moments. These forces and moments are found as

$$X^* = X_u u + X_v v + X_w w + X_p p + X_q q + X_r r + X_{uu} u^2 + X^{ST}, \tag{25}$$

$$Y^* = Y_u u + Y_v v + Y_w w + Y_p p + Y_q q + Y_r r + Y^{ST}, \tag{26}$$

$$Z^* = Z_u u + Z_v v + Z_w w + Z_p p + Z_q q + Z_r r + Z_z z + Z_\varphi \varphi + Z_\theta \theta + Z^{ST}, \tag{27}$$

$$K^* = K_u u + K_v v + K_w w + K_p p + K_q q + K_r r + K_z z + K_\varphi \varphi + K_\theta \theta + K^{ST}, \tag{28}$$

$$M^* = M_u u + M_v v + M_w w + M_p p + M_q q + M_r r + M_z z + M_\varphi \varphi + M_\theta \theta + M^{ST}, \tag{29}$$

$$N^* = N_u u + N_v v + N_w w + N_p p + N_q q + N_r r + N^{ST}, \tag{30}$$

In the above equations (Eqs. (24) to (30), forces (X, Y and Z) or moments (K, M and N) with acceleration subscripts (like $\dot u$) refer to added mass coefficients. Forces or moments with velocity subscripts (like u) denote the damping coefficients. Forces (or moments) with subscripts of z, φ, and θrefer to hydrostatic restoring forces (or moments) caused by heave, roll and pitch. Any force or moment with an ST superscript shows the steady hydrodynamic moments. Equations for determination of all added mass coefficients, damping coefficients, steady forces, and restoring hydrostatic forces are presented in appendices B, C, D and E respectively.

3. Guideline for simulation

To simulate the problem, the craft is initially located at the origin of the earth-fixed coordinate system. The initial surge speed is set to be equal to the speed of the craft, and other velocities are set to be zero at $t = 0$. The initial trim angle and heave of the vessel are set to be equal to running attitudes of the vessel in the calm water condition (Ghadimi et al., 2016c). The initial roll and yaw angles of the vessel are set to be

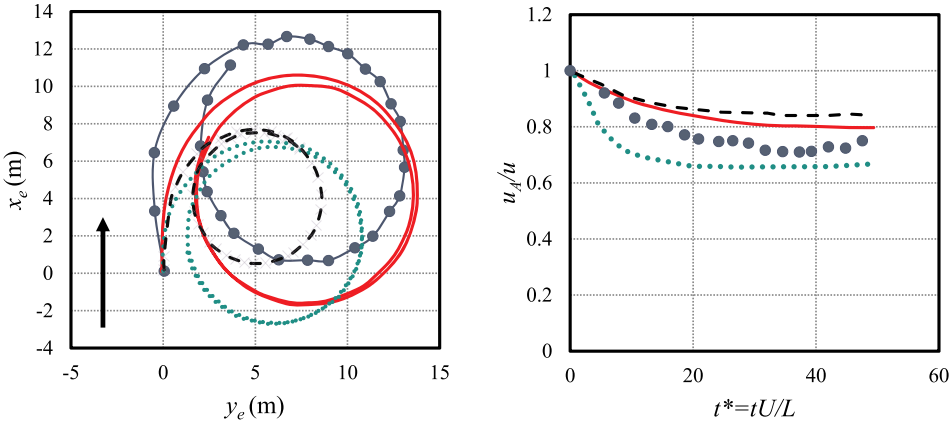

Fig. 5. Comparison of 2D + T results (solid red) against experimental data (blue circles) of Katayama et al. (2006), conventional method (dashed black), and interpolation method (dotted green) in steady turning with $\delta = 20$ at $Fn_B = 2.13$: (a) trajectory of the vessel and (b) speed reduction. The black arrow shows the initial direction of the motion of the vessel. (For interpretation of the references to colour in this figure legend, the reader is referred to the Web version of this article.)

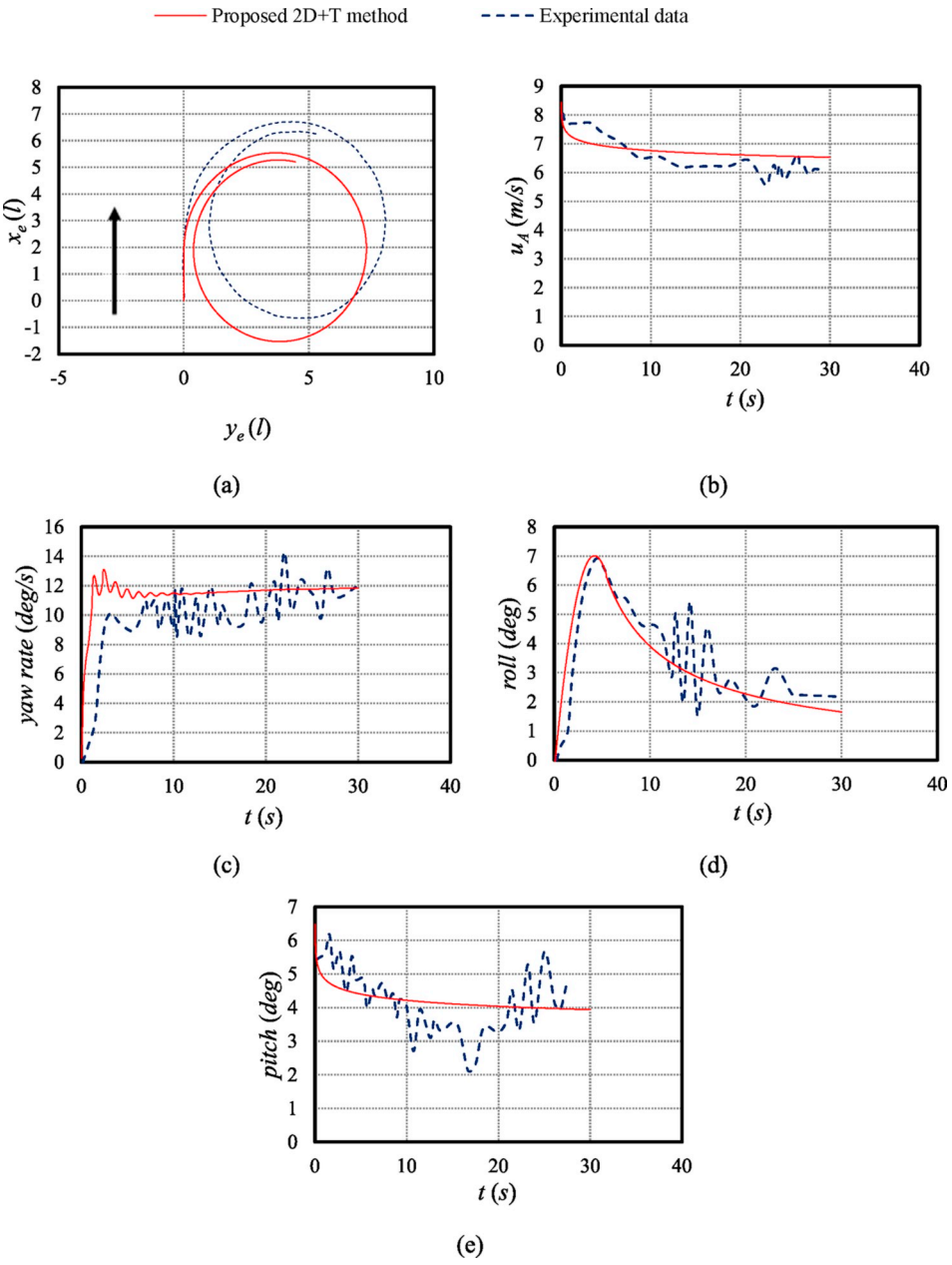

Fig. 6. Comparison of predicted results against experimental data of Kim and Kim (2017) in steady turning with $\delta = 15$ at $u = 7.71$ m/s: (a) trajectory of the vessel, (b) speed reduction, (c) yaw rate, (d) roll angle, and (e) pitch angle. The black arrow shows the initial direction of the motion of the vessel.

zero. An unknown variable vector is defined as

$$\boldsymbol{\eta} = [u \quad v \quad w \quad p \quad q \quad r] \tag{31}$$

Forces (in the hydrodynamic frame) are found at each time step. A Runge-Kutta method (like the one used in Ghadimi et al., 2016b) is used to numerically solve the problem in the time domain. At each time step, accelerations (the $\dot{\boldsymbol{\eta}}$ vector) are computed. Then, the $\boldsymbol{\eta}$ vector is found. In the next step, the velocities of the vessel in the earth-fixed coordinate system are computed by,

$$\boldsymbol{x}_e = \begin{bmatrix} \cos\theta\cos\psi & -\cos\varphi\sin\psi + \sin\varphi\sin\theta\cos\psi & \sin\varphi\sin\psi + \cos\varphi\sin\theta\cos\psi \\ \cos\theta\sin\psi & \cos\varphi\cos\psi + \sin\varphi\sin\theta\sin\psi & -\sin\varphi\cos\psi + \cos\varphi\sin\theta\sin\psi \\ -\sin\theta & \sin\varphi\cos\theta & \cos\varphi\cos\theta \end{bmatrix} \begin{bmatrix} u \\ v \\ w \end{bmatrix} \tag{32}$$

$$\Omega_e = \begin{bmatrix} 1 & \sin\varphi\tan\theta & \cos\varphi\tan\theta \\ 0 & \cos\varphi & -\sin\varphi \\ 0 & \sin\varphi\sec\theta & \cos\varphi\sec\theta \end{bmatrix} \begin{bmatrix} p \\ q \\ r \end{bmatrix} \tag{33}$$

Finally, the position of the vessel in the earth fixed frame is found. Then, computations of the next time step are performed. Note that the thrust angle is set to be equal to a constant value during the simulation and no artificial restoring force or moment for sway and yaw motions is considered.

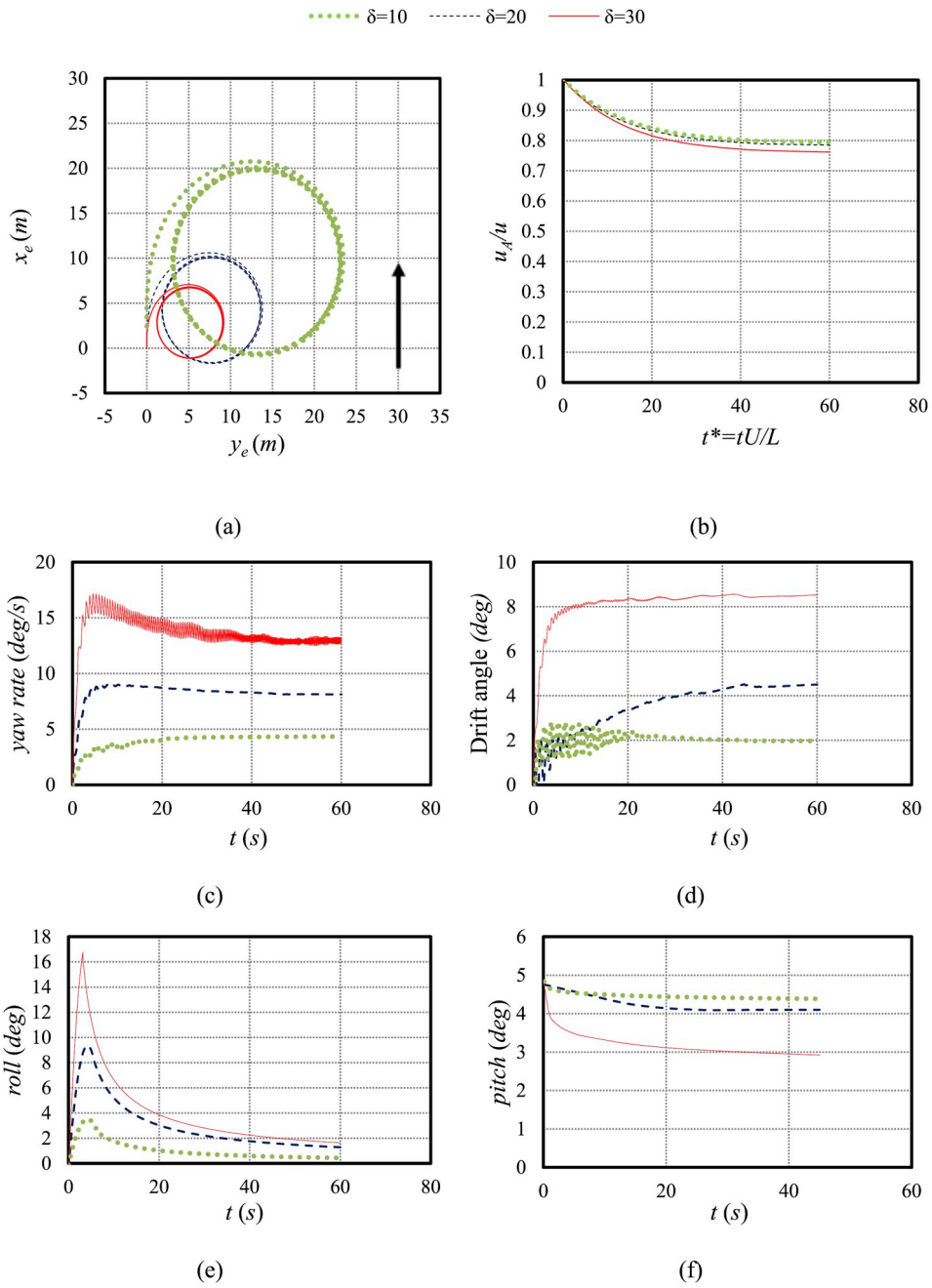

Fig. 7. Simulation of turning motion of the considered planing hull with three different δ at beam Froude Number of 2.13: (a) trajectory of the vessel, (b) speed reduction, (c) yaw rate, (d) drift angle, (e) yaw rate, (e) roll angle and (f) pitch angle. The black arrow shows the initial direction of the motion of the vessel.

4. Results

4.1. Comparative analysis

To explore the validity of the developed 2D + T method, the mathematical results (of the 2D + T method) have been compared against the results of previous experimental studies. One of these studies was conducted by Katayama et al. (2006) and the other was performed by Kim and Kim (2017). Principal characteristics of these planing hulls (studied by these authors) are illustrated in Table 1.

Results (computed by the 2D + T theory) of turning simulation (including the rajectory of the vessel and speed reduction) of the planing craft studied by Katayama et al. (2006) are presented in Fig. 5. Simulations are performed for the thrust angle of $\delta = 20^\circ$ at beam Froude Number of 2.13. Experimental results (blue circles with solid line) of Katayama et al. (2006) are also presented in this figure. Moreover, the results of two other simulations, both of which were performed by Katayama et al. (2006) are reported. First simulation (dashed black) was performed using a conventional method by Katayama et al. (2006). The other (dotted green) was performed using an interpolation method (which uses the instant hydrodynamic coefficient of the vessel) by Katayama et al. (2006).

The trajectory curve (Fig. 5a) shows that the 2D + T theory predicts the turning radius with proper accuracy. 2D + T method predicts the turning radius to be 6.1 *m* and the experimentally measured turning radius is 5.8 *m*. Conventional method and interpolation method underpredict the turning radius of the planing hull. 2D + T method predicts a smaller advance, i.e., the turning is shifted backward (in comparison with experimentally measured turning circle). Also, a larger transit is predicted by the 2D + T theory (turning circle is shifted toward the right

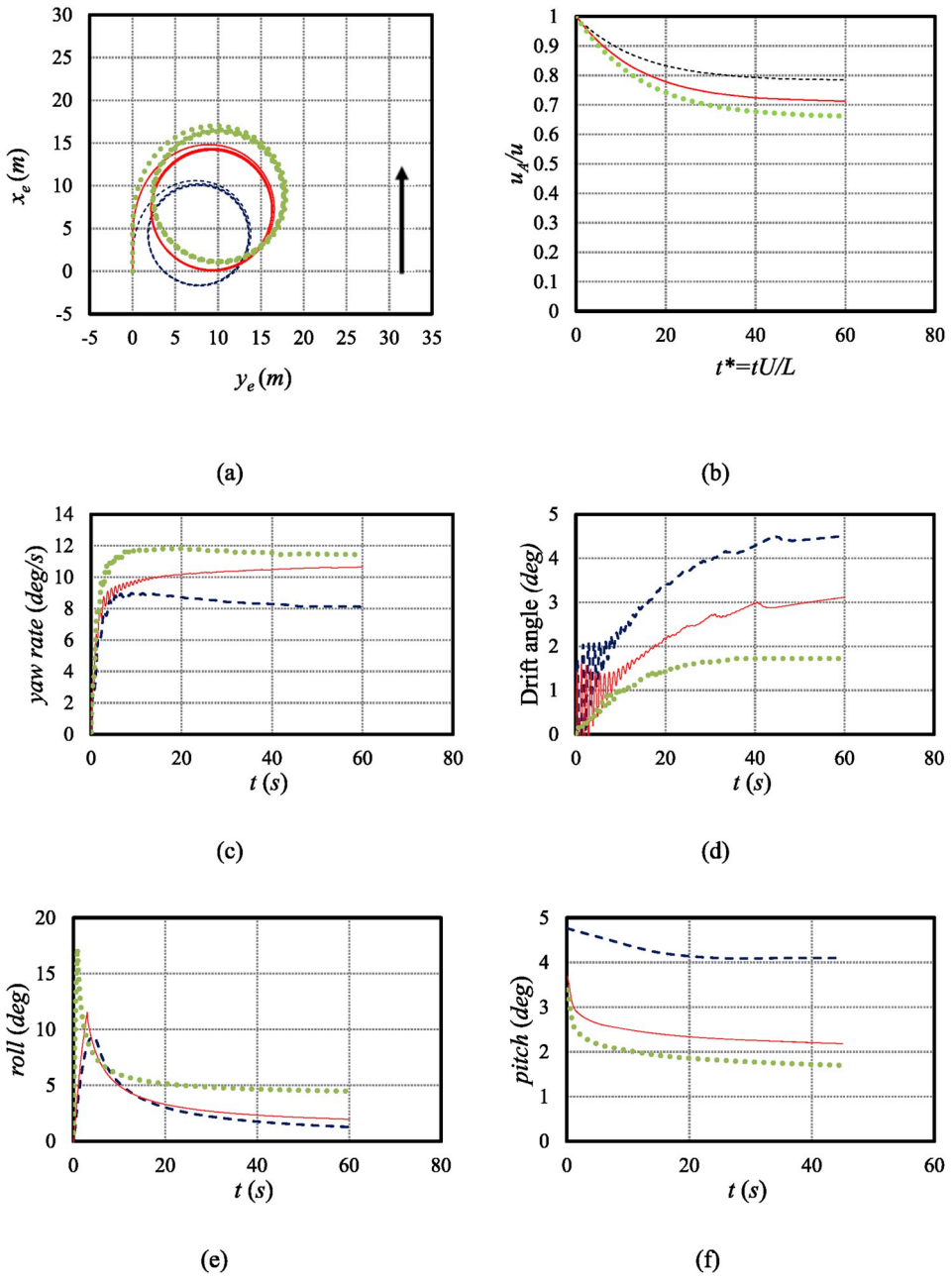

Fig. 8. Simulation of turning motion of the considered planing hull with $\delta = 20°$ at beam Froude Numbers of 2.13 (dashed black), 2.63 (solid red) and 3.13 (dotted green): (a) trajectory of the vessel, (b) speed reduction, (c) yaw rate, (d) drift angle, (e) yaw rate, (e) roll angle and (f) pitch angle. The black arrow shows the initial direction of the motion of the vessel. (For interpretation of the references to colour in this figure legend, the reader is referred to the Web version of this article.)

side). The possible reason of this error in prediction of the transit and advance of the vessel is the initial conditions of the vessel (in the laboratory test) we are not sure about. But, the proper accuracy of the 2D + T theory in the prediction of the turning radius shows that this method (2D + T) provides hydrodynamic forces (including added mass, damping and steady turning forces) with proper accuracy.

The speed reduction curve (time history of u_A/u) shows that 2D + T method provides similar results (not absolutely) to experimental data. At the final stage of simulations, the experimentally measured value of u_A/u is found to be 0.72.2D + T method predicts the u_A/u to be 0.79 at the end. Conventional and interpolation methods respectively over-predict and under-predict u_A/u. But, the accuracy of the interpolation method is better than the conventional method.

Fig. 6 presents the comparison of the predicted results (by 2D + T method) against experimental data of Kim and Kim (2017) who provided time history of pitch and roll angles (in addition to the trajectory of the vessel). The craft is supposed to turn with a speed of 7.71 m/s and δ=15°. The comparison of the trajectory curves shows that the current simulation (solid red) predicts the turning radius with relatively good accuracy (note that the error in prediction of the turning radius is 5.8%). The trajectory of the vessel is shifted backward 1.2 m, which means the advance and transit of the vessel are not predicted with proper accuracy. Note that, we are not sure about the initial conditions of the experimental tests which can highly affect these two values. Time history of speed reduction (Fig. 6b) of both 2D + T simulation and experiment show similarities. The final speed of the vessel in the steady phase is predicted by an error of 11.2%. Some fluctuations (sudden jumps) can be seen in the measurements, which cannot be computed by the 2D + T method. These fluctuations can be attributed to a real craft and real condition of the sea (which is not considered in the current

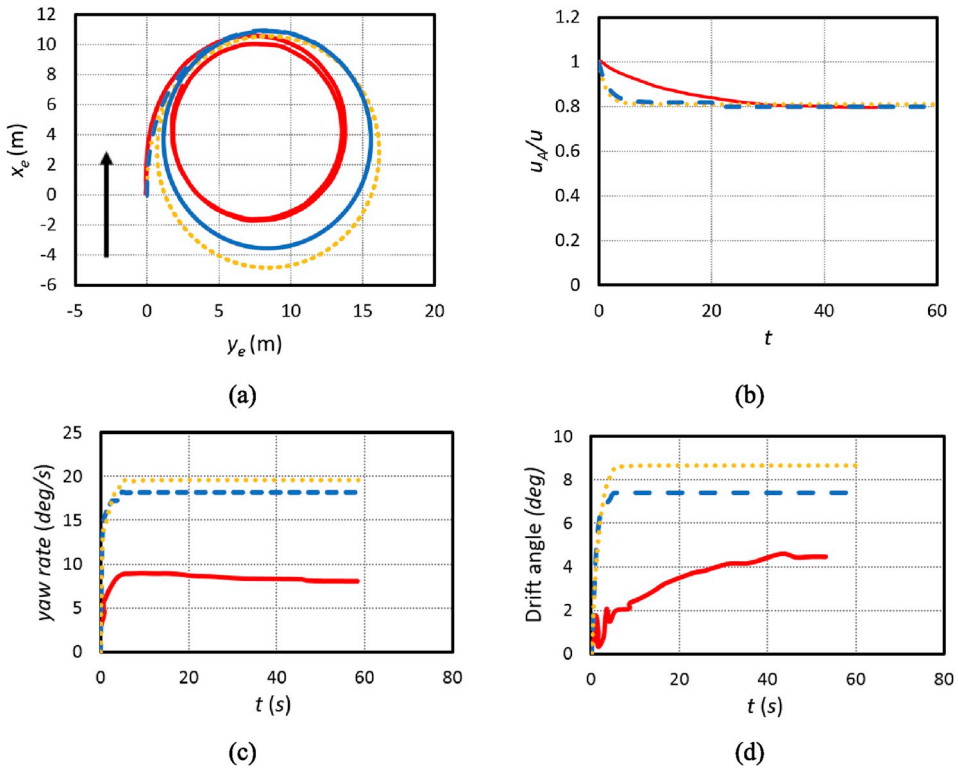

Fig. 9. Simulation of turning motion of the considered planing hull with $\delta = 20^\circ$ at beam Froude Number of 2.13 for 6DOF (solid red), 4DOF (dashed blue) and 3DOF (dotted orange): (a) trajectory of the vessel, (b) speed reduction, (c) yaw rate, (d) drift angle. The black arrow shows the initial direction of the motion of the vessel. (For interpretation of the references to colour in this figure legend, the reader is referred to the Web version of this article.)

model since water is assumed to be perfectly calm).

The time history of the yaw rate can be seen in Fig. 6c. The steady yaw rate of the 2D + T simulation (11.8° per second) almost agrees with the mean value (11.17° per second) of the measurements (measurements show some fluctuations 2D + T theory cannot model). There are some differences between the results (of the 2D + T method and experiments) at the early stage of the turning. For example, the measured yaw rate is seen to reach its peak at t = 3.2 s. But, 2D + T results show that this peak occurs slightly sooner (1 s). Note that, we are sure about the maximum thrust inclination angle (in sea trials), but we are not sure about the time history of the thrust inclination angle. This angle is initially set to be 15° in simulations. One possible reason for this difference between the peak time (the time at which the yaw rate reaches its maximum value) is the uncertainty about the initial value of the thrust inclination angle in sea trials.

The time history of the mathematically predicted roll angle is in good agreement with the time history of the experimentally measured roll angle (Fig. 6d). Predicted roll angle reaches its maximum value at $t = 4.3$ s, then its value highly decreases and becomes smaller than 2°. Some fluctuations can be seen in the experimentally measured time history of the roll motion. Finally, the predicted pitch vs. time curves of the simulations and measurements show similarities. At the beginning of the turning motion, their values decrease and then converge to a constant value (for the case of experiments, the final value refers to the time average of the pitch after the unsteady motion). It should be noted that the experimental data fluctuate for different reasons such as the vibration of the body, however, the current method cannot model fluctuations.

4.2. Effects of parameters

Using the current mathematical model, effects of speed and

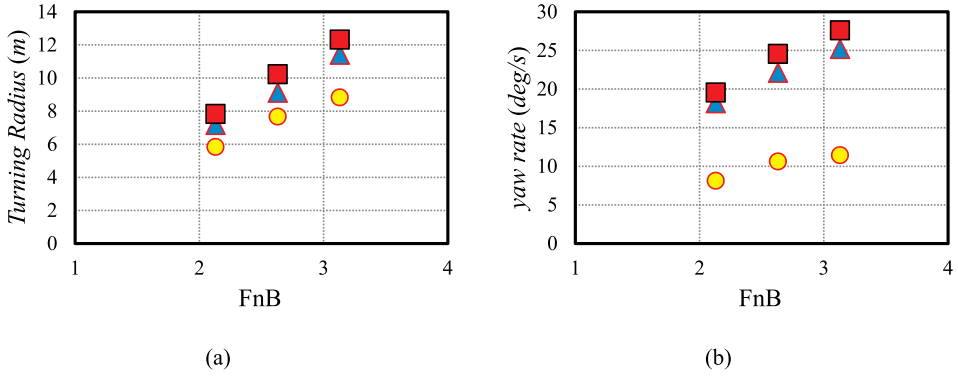

Fig. 10. Effects of the degrees of freedom on the turning radius (a) and yaw rate of the vessel (b). Results are related to the planing model studied by Katayama et al. (2006). Circles, triangles and squares respectively refer to the 6DOF, 4DOF and 3DOF cases.

inclination angle of thrust force on the motion of a planing hull in steady turning have been investigated. Simulations were performed to model the planing hull studied by Katayama et al. (2006).

Fig. 7 shows the results of simulation at three different thrust angles, $\delta = 10$, 20 and 30° at the beam Froude Number of 2.13. The turning radius of the vessel is seen to decrease by the increase in δ. Speed reduction becomes more significant by the increase in δ. Larger inclination angle leads to larger force in sway direction and smaller force in surge direction, causing more reduction in speed.

The yaw rate of the vessel becomes larger with the increase in δ (Fig. 7c). On the other hand, the drift angle increases with the increase in δ. The roll angle of the vessel increases and reaches a peak and then decreases and finally converges. The peak roll highly increases with the increase in δ. At the steady state condition, when the roll angle converges to a constant value, the effects of δ on roll angle vanish. For example, the maximum roll angle at $\delta = 10$ and 30° are 4.4 and 17.2°, respectively. But, the steady roll angles are 1.4 and 3.8° at $\delta = 10$ and 30°. Under the action of yaw and sway speeds, larger angular moments (Izadi et al. 2018), as it was seen in formulated equations (see equation (29)), act on the vessel. Therefore, at a very early stage of turning, when instantaneous speeds are larger (compare to the steady state condition), surge and sway speed lead in a larger exciting moment in the roll direction. When the vessel reaches the steady state condition, surge and sway speed decrease. Their influences on roll angle are reduced compared with the early stage of turning. Finally, the pitch angle of the vessel decreases in all cases. However, this decrease is larger when δ is larger.

Simulations (performed by 2D + T method) of turning motion of the considered planing hull with $\delta = 20°$ at three different beam Froude Numbers of 2.13, 2.63 and 3.13 are displayed in Fig. 8. Larger speed has a larger turning radius (Fig. 8a). Speed reduction becomes more significant as the beam Froude Number increases (Fig. 8b). The results of the yaw rate also indicate that an increase in speed increases the yaw rate (Fig. 8c). The drift angle of the vessel becomes smaller with the increase in speed (Fig. 8d). When the speed of the vessel becomes larger, the angle between sway speed and surge speed becomes smaller. According to the results presented for the roll angle (Fig. 8d), peak roll increases by the increase in speed, and the final heel angle of the vessel is larger when speed is larger (Fig. 8e). At higher speeds, the wetted surface of the craft becomes lesser and the contribution of the hydrostatic force thereby reduces (Esfandiari et al., 2019). Moreover, the pitch angle is reduced by the increase in speed (Fig. 8f). It is obvious that dynamic trim angle of a vessel becomes smaller when speed becomes larger (Ghadimi et al., 2015).

4.3. Effects of degrees of freedom on the turning simulation

The effects of degrees of freedom on steady turning motion of the planing hull are studied. Simulation of the turning motion of the model studied by Katayama et al. (2006) is performed for 6DOF, 4DOF (surge, sway, roll and yaw) and 3DOF (surge, sway and yaw) cases at beam Froude number of 2.13 (inoculation angle of thrust is set to be 20°). Results are presented in Fig. 9, showing that the number of degrees of freedom can affect the results.

The turning radius of the vessel becomes larger by the decrease in degrees of freedom (Fig. 9a). When the degrees of freedom are less, the contribution of heave and pitch motions (as well as roll motion for the case of 3DOF motion) becomes less. Therefore, smaller forces act on the bottom of the vessel, allowing it to travel in a larger loop (larger circle) during the turning motion. Speed reduction (Fig. 9b) of the boat is found to be the same (at the final time) for all cases. This point shows that heave, pitch and roll forces do not lead to any significant surge force during the steady turning. But, at the early stage of turning, the speed reduction is larger for the cases with smaller degrees of freedom (see the first 20 s of the simulations). The different behavior at the early stage of the turning can be attributed to extra damping forces in heave direction which disappear when turning motion becomes steady (Tavakoli et al., 2018). Yaw rate of the vessel (Fig. 9c), as well as its drift angle (Fig. 9d) are smaller when the vessel is free in all six degrees of freedom. For the cases of 4DOF and 3DOF simulations, the vessel travels in the horizontal plane with larger yaw rates, which result in larger turning circles. This fact shows that, when the vessel is free in all degrees of freedom, contributions of heave and pitch motions in yaw direction resist against the increase in the yaw moment (and thus the vessel has smaller yaw acceleration and yaw rate).

The effects of degrees of freedom on the turning motion of the vessel are studied at beam Froude Numbers of 2.63 and 3.13. Fig. 10 shows the turning radius and (steady) yaw rate of the vessel studied by Katayama for three different cases (6DOF, 4DOF and 3DOF) at the mentioned Froude Numbers. Results presented in this figure show that the turning radius (Fig. 10a) and the yaw rate of the vessel (Fig. 10b) increases by the decrease in the degrees of freedom at all considered speeds.

5. Conclusions

A mathematical simulation for the turning motion of a planing hull was developed using 2D + T theory by coupling all six degrees of motion. Sectional hydrodynamic and hydrostatic forces and moments were found by using water entry of a solid wedge section. Extending 2D forces and moments over the length of the craft, equations for maneuvering forces and moments involving in turning were developed. Added mass, damping, steady maneuvering, and hydrostatic restoring forces and moments were found.

Firstly, the results of the current method were compared against two of previous experiments. It was seen that 2D + T method predicted the turning radius as well as the trajectory of the vessel with reasonable accuracy. Also, it was seen that time histories of pitch and roll angles were predicted with reasonable accuracy. The behavior of the vessel during the turning motion was also investigated. It was seen that the turning diameter of the vessel decreases by the increase in thrust angle. Also, speed reduction, yaw rate, and the drift angle were found to become larger when the thrust angle increases. In addition to these, it was shown that, roll angle is larger when the thrust angle is larger. It was seen that the turning radius and maximum roll angle of the craft increase while drift and pitch angles become smaller as speed increases. The effects of degrees of freedom on the turning motion were studied. It was demonstrated that, when the vessel is not allowed to have motions in heave, pitch and roll directions, turning radius and yaw rate increase.

It is anticipated that future research may provide mathematical models for active control of planing craft in turning motion. Moreover, authors are seeking for new theoretical solutions for water entry, by which they can increase the accuracy of the method, especially at high yaw angles.

Acknowledgement

ST is supported by a Melbourne Research Scholarship (MRS) awarded by the University of Melbourne.

Appendix A. Half-wetted beam

Half-wetted beam and asymmetric parameter of the vessel are computed by using the values of half-wetted beam of starboard (c_1) and half-wetted beam of port (c_2) as

$$c = \frac{(c_1 + c_2)}{2} \tag{A.1}$$

$$\mu = \frac{(c_1 - c_2)}{2} \tag{A.2}$$

c_i(half wetted beam at side i) is computed using

$$c_i = \left(\frac{\pi}{2} - \beta_i\left(1 - \frac{2}{\pi}\right)\right)\left(\frac{d}{\tan\beta_i}\right) \tag{A.3}$$

when chine is dry. Here d is water draft at the section. As water reaches the chine, half wetted beam is computed by

$$c_i = b_i \tag{A.4}$$

where b_i is the half beam as is found by

$$b_i = \frac{B}{2}\frac{\cos\beta_i}{\cos\beta} \tag{A.5}$$

Appendix B. Added mass coefficients

Added mass coefficients are found using the following equations.

$$X_{\dot{u}} = -\left(M_{\chi\xi}\sin\psi\sin\theta + M_{\chi\chi}\sin^2\psi + M_{\xi\chi}\sin\psi\sin\theta + M_{\xi\xi}\sin^2\theta\right) \tag{B.1}$$

$$X_{\dot{v}} = -\left(M_{\chi\chi}\cos\psi\sin\psi + M_{\xi\chi}\cos\psi\sin\theta\right) \tag{B.2}$$

$$X_{\dot{w}} = -\left(M_{\chi\xi}\cos\theta\sin\psi + M_{\xi\xi}\cos\theta\sin\theta\right) \tag{B.3}$$

$$X_{\dot{p}} = -\left(M_{\chi\phi}\sin\psi + M_{\xi\phi}\sin\theta\right) \tag{B.4}$$

$$X_{\dot{q}} = Q_{\chi\xi}\sin\psi + Q_{\xi\xi}\sin\theta \tag{B.5}$$

$$X_{\dot{r}} = Q_{\chi\chi}\sin\psi + Q_{\xi\chi}\sin\theta \tag{B.6}$$

$$Y_{\dot{u}} = -\left(M_{\chi\xi}\sin\theta\cos\psi + M_{\chi\chi}\sin\psi\cos\psi\right) \tag{B.7}$$

$$Y_{\dot{v}} = -M_{\chi\chi}\cos^2\psi \tag{B.8}$$

$$Y_{\dot{w}} = -M_{\chi\xi}\cos\theta\cos\psi \tag{B.9}$$

$$Y_{\dot{p}} = -M_{\chi\phi}\cos\psi \tag{B.10}$$

$$Y_{\dot{q}} = Q_{\chi\xi}\cos\psi \tag{B.11}$$

$$Y_{\dot{r}} = Q_{\chi\chi}\cos\psi \tag{B.12}$$

$$Z_{\dot{u}} = -\left(M_{\xi\chi}\sin\psi\cos\theta + M_{\xi\xi}\sin\theta\cos\theta\right) \tag{B.13}$$

$$Z_{\dot{v}} = -M_{\xi\chi}\cos\psi\cos\theta \tag{B.14}$$

$$Z_{\dot{w}} = -M_{\xi\xi}\cos^2\theta \tag{B.15}$$

$$Z_{\dot{p}} = -M_{\xi\phi}\cos\theta \tag{B.16}$$

$$Z_{\dot{q}} = Q_{\xi\xi}\cos\theta \tag{B.17}$$

$$Z_{\dot{r}} = Q_{\xi\chi}\cos\theta \tag{B.18}$$

$$K_{\dot{u}} = -\left(M_{\phi\chi}\sin\psi + M_{\phi\xi}\sin\theta\right) \tag{B.19}$$

$$K_{\dot{v}} = -M_{\phi\chi}\cos\psi \tag{B.20}$$

$$K_{\dot{w}} = -M_{\phi\xi}\cos\theta \tag{B.21}$$

$$K_{\dot{p}} = -M_{\phi\phi} \tag{B.22}$$

$$K_{\dot{q}} = Q_{\phi\xi} \tag{B.23}$$

$$K_{\dot{r}} = Q_{\phi\chi} \tag{B.24}$$

$$M_{\dot{u}} = Q_{\xi\chi}\sin\psi + Q_{\xi\xi}\sin\theta \tag{B.25}$$

$$M_{\dot{v}} = Q_{\xi\chi}\cos\psi \tag{B.26}$$

$$M_{\dot{w}} = Q_{\xi\xi}\cos\theta \tag{B.27}$$

$$M_{\dot{p}} = Q_{\xi\phi} \tag{B.28}$$

$$M_{\dot{q}} = -I_{\xi\xi} \tag{B.29}$$

$$M_{\dot{r}} = -I_{\xi\chi} \tag{B.30}$$

$$N_{\dot{u}} = Q_{\chi\xi}\sin\theta + Q_{\chi\chi}\sin\psi \tag{B.31}$$

$$N_{\dot{v}} = Q_{\chi\chi}\cos\psi \tag{B.32}$$

$$N_{\dot{w}} = Q_{\chi\xi}\cos\theta \tag{B.33}$$

$$N_{\dot{p}} = Q_{\chi\phi} \tag{B.34}$$

$$N_{\dot{q}} = -I_{\chi\xi} \tag{B.35}$$

$$N_{\dot{r}} = -I_{\chi\chi} \tag{B.36}$$

Appendix C. Damping coefficients

Damping coefficients are found using the following equations.

$$X_u = \begin{pmatrix} -\left(\int_L R(x)\sin\theta\dot{m}_{\chi\xi}dx\right) - um_{\chi\xi}\sin\theta| \\ -\left(\int_L R(x)\sin\psi\dot{m}_{\chi\chi}dx\right) - um_{\chi\chi}\sin\psi|_{x=x_T} \end{pmatrix}\sin\psi + + \begin{pmatrix} -\left(\int_L R(x)\sin\theta\dot{m}_{\xi\xi}dx\right) - um_{\xi\xi}\sin\theta|_{x=x_T} \\ -\left(\int_L R(x)\sin\psi\dot{m}_{\xi\chi}dx\right) - um_{\xi\chi}\sin\psi|_{x=x_T} \end{pmatrix}\sin\theta \tag{C.1}$$

$$X_v = \left(-\left(\int_L R(x)\cos\psi\dot{m}_{\chi\chi}dx\right) - um_{\chi\chi}\cos\psi|_{x=x_T}\right)\sin\psi + \left(-\left(\int_L R(x)\cos\psi\dot{m}_{\xi\chi}dx\right) - um_{\xi\chi}\cos\psi|_{x=x_T}\right)\sin\theta \tag{C.2}$$

$$X_w = \left(-\left(\int_L R(x)\cos\theta\dot{m}_{\chi\xi}dx\right) - um_{\chi\xi}\cos\theta|_{x=x_T}\right)\sin\psi + \left(-\left(\int_L R(x)\cos\theta\dot{m}_{\xi\xi}dx\right) - um_{\xi\xi}cos\theta|_{x=x_T}\right)\sin\theta \tag{C.3}$$

$$X_p = \left(-\left(\int_L R(x)\dot{m}_{\chi\phi}dx\right) - um_{\chi\phi}|_{x=x_T}\right)\sin\psi + \left(-\left(\int_L R(x)\dot{m}_{\xi\phi}dx\right) - um_{\xi\phi}|_{x=x_T}\right)\sin\theta \tag{C.4}$$

$$X_q = \left(-\left(\int_L R(x)\dot{m}_{\chi\xi}xdx\right) - xum_{\chi\xi}|_{x=x_T}\right)\sin\psi - \left(\left(\int_L R(x)\dot{m}_{\xi\xi}xdx\right) - xum_{\xi\xi}|_{x=x_T}\right)\sin\theta \tag{C.5}$$

$$X_r = -\left(-\left(\int_L R(x)\dot{m}_{\chi\chi}xdx\right) - xum_{\chi\chi}|_{x=x_T}\right)sin\,\psi - \left(-\left(\int_L R(x)\dot{m}_{\xi\chi}xdx\right) - xum_{\xi\chi}|_{x=x_T}\right)sin\,\theta \tag{C.6}$$

$$X_{uu} = \frac{1}{2}\rho S\left(C_f + \Delta C_f\right) + \frac{1}{2}\rho C_{DT}A_T \tag{C.7}$$

$$Y_u = \begin{pmatrix} -\left(\int_L R(x)\sin\theta\dot{m}_{\chi\xi}dx\right) - um_{\chi\xi}\sin\theta|_{x=x_T} \\ -\left(\int_L R(x)\sin\psi\dot{m}_{\chi\chi}dx\right) - um_{\chi\chi}\sin\psi|_{x=x_T} \end{pmatrix}\cos\psi \tag{C.8}$$

$$Y_v = \left(-\left(\int_L R(x)\cos\psi\dot{m}_{\chi\chi}dx\right) - um_{\chi\chi}\cos\psi|_{x=x_T}\right)\cos\psi \tag{C.9}$$

$$Y_w = \left(-\left(\int_L R(x)\cos\theta\dot{m}_{\chi\xi}dx\right) - um_{\chi\xi}\cos\theta|_{x=x_T}\right)\cos\psi \tag{C.10}$$

$$Y_p = \left(-\left(\int_L R(x)\dot{m}_{\chi\phi}dx \right) - um_{\chi\phi}|_{x=x_T} \right)\cos\psi \tag{C.11}$$

$$Y_q = -\left(-\left(\int_L R(x)\dot{m}_{\chi\xi}xdx \right) - xum_{\chi\xi}|_{x=x_T} \right)\cos\psi \tag{C.12}$$

$$Y_r = -\left(-\left(\int_L R(x)\dot{m}_{\chi\chi}xdx \right) - xum_{\chi\chi}|_{x=x_T} \right)\cos\psi \tag{C.13}$$

$$Z_u = \begin{pmatrix} -\left(\int_L R(x)\sin\theta\dot{m}_{\xi\xi}dx \right) - um_{\xi\xi}\sin\theta|_{x=x_T} \\ -\left(\int_L R(x)\sin\psi\dot{m}_{\xi\chi}dx \right) - um_{\xi\chi}\sin\psi|_{x=x_T} \end{pmatrix}\cos\theta \tag{C.14}$$

$$Z_v = \left(-\left(\int_L R(x)\cos\psi\dot{m}_{\xi\chi}dx \right) - um_{\xi\chi}\cos\psi|_{x=x_T} \right)\cos\theta \tag{C.15}$$

$$Z_w = \left(-\left(\int_L R(x)\cos\theta\dot{m}_{\xi\xi}dx \right) - um_{\xi\xi}\cos\theta|_{x=x_T} \right)\cos\theta \tag{C.16}$$

$$Z_p = \left(-\left(\int_L R(x)\dot{m}_{\xi\phi}dx \right) - um_{\xi\phi}|_{x=x_T} \right)\cos\theta \tag{C.17}$$

$$Z_q = -\left(-\left(\int_L R(x)\dot{m}_{\xi\xi}xdx \right) - xum_{\xi\xi}|_{x=x_T} \right)\cos\theta \tag{C.18}$$

$$Z_r = -\left(-\left(\int_L R(x)\dot{m}_{\xi\chi}xdx \right) - xum_{\xi\chi}|_{x=x_T} \right)\cos\theta \tag{C.19}$$

$$K_u = \begin{pmatrix} -\left(\int_L R(x)\sin\theta\dot{m}_{\phi\xi}dx \right) - um_{\phi\xi}\sin\theta|_{x=x_T} \\ -\left(\int_L R(x)\sin\psi\dot{m}_{\phi\chi}dx \right) - um_{\phi\chi}\sin\psi|_{x=x_T} \end{pmatrix} \tag{C.20}$$

$$K_v = \left(-\left(\int_L R(x)\cos\psi\dot{m}_{\phi\chi}dx \right) - um_{\varphi\chi}\cos\psi|_{x=x_T} \right) \tag{C.21}$$

$$K_w = \left(-\left(\int_L R(x)\cos\theta\dot{m}_{\phi\xi}dx \right) - um_{\phi\xi}\cos\theta|_{x=x_T} \right) \tag{C.22}$$

$$K_p = \left(-\left(\int_L R(x)\dot{m}_{\phi\phi}dx \right) - um_{\phi\phi}|_{x=x_T} \right) \tag{C.23}$$

$$K_q = -\left(-\left(\int_L R(x)\dot{m}_{\phi\xi}xdx \right) - xum_{\phi\xi}|_{x=x_T} \right) \tag{C.24}$$

$$K_r = -\left(-\left(\int_L R(x)\dot{m}_{\phi\chi}xdx \right) - xum_{\phi\chi}|_{x=x_T} \right) \tag{C.25}$$

$$M_u = \begin{pmatrix} -\left(\int_L R(x)\sin\theta\dot{m}_{\xi\xi}xdx \right) - xum_{\xi\xi}\sin\theta|_{x=x_T} \\ -\left(\int_L R(x)\sin\psi\dot{m}_{\xi\chi}xdx \right) - xum_{\xi\chi}\sin\psi|_{x=x_T} \end{pmatrix} \tag{C.26}$$

$$M_v = \left(-\left(\int_L R(x)\cos\psi\dot{m}_{\xi\chi}xdx \right) - xum_{\xi\chi}\cos\psi|_{x=x_T} \right) \tag{C.27}$$

$$M_w = \left(-\left(\int_L R(x)\cos\theta\dot{m}_{\xi\xi}xdx \right) - xum_{\xi\xi}\cos\theta|_{x=x_T} \right) \tag{C.28}$$

$$M_p = \left(-\left(\int_L R(x)\dot{m}_{\xi\phi} x dx \right) - x u m_{\xi\phi}|_{x=x_T} \right) \tag{C.29}$$

$$M_p = -\left(-\left(\int_L R(x)\dot{m}_{\xi\xi} x^2 dx \right) - x^2 u m_{\xi\xi}\big|_{x=x_T} \right) \tag{C.30}$$

$$M_r = -\left(-\left(\int_L R(x)\dot{m}_{\xi\chi} x^2 dx \right) - x^2 u m_{\xi\chi}|_{x=x_T} \right) \tag{C.31}$$

$$N_u = \begin{pmatrix} -\left(\int_L R(x)\sin\theta \dot{m}_{\chi\xi} x dx \right) - x u m_{\chi\xi} \sin\theta|_{x=x_T} \\ -\left(\int_L R(x)\sin\psi \dot{m}_{\chi\chi} x dx \right) - x u m_{\chi\chi} \sin\psi|_{x=x_T} \end{pmatrix} \tag{C.32}$$

$$N_v = \left(-\left(\int_L R(x)\cos\psi \dot{m}_{\chi\chi} x dx \right) - x u m_{\chi\chi} \cos\psi|_{x=x_T} \right) \tag{C.33}$$

$$N_w = \left(-\left(\int_L R(x)\cos\theta \dot{m}_{\chi\xi} x dx \right) - x u m_{\chi\xi} \cos\theta|_{x=x_T} \right) \tag{C.34}$$

$$N_p = \left(-\left(\int_L R(x)\dot{m}_{\chi\phi} x dx \right) - x u m_{\chi\phi}|_{x=x_T} \right) \tag{C.35}$$

$$N_q = -\left(-\left(\int_L R(x)\dot{m}_{\chi\xi} x^2 dx \right) - x^2 u m_{\chi\xi}\big|_{x=x_T} \right) \tag{C.36}$$

$$N_r = -\left(-\left(\int_L R(x)\dot{m}_{\chi\chi} x^2 dx \right) - x^2 u m_{\chi\chi}|_{x=x_T} \right) \tag{C.37}$$

Appendix D. Steady forces and moments

Steady forces and moments of manoeuvring are found by

$$X^{ST} = \begin{pmatrix} (M_{\chi\xi} q(w\sin\theta - u\cos\theta) + M_{\chi\chi} r(w\sin\psi - u\cos\psi))\sin\psi \\ (M_{\xi\xi} q(w\sin\theta - u\cos\theta) + M_{\xi\chi} r(w\sin\psi - u\cos\psi))\sin\theta \end{pmatrix} \tag{D.1}$$

$$Y^{ST} = (M_{\chi\xi} q(w\sin\theta - u\cos\theta) + M_{\chi\chi} r(w\sin\psi - u\cos\psi))\cos\psi \tag{D.2}$$

$$Z^{ST} = (M_{\xi\xi} q(w\sin\theta - u\cos\theta) + M_{\xi\chi} r(w\sin\psi - u\cos\psi))\cos\theta \tag{D.3}$$

$$K^{ST} = (M_{\varphi\xi} q(w\sin\theta - u\cos\theta) + M_{\varphi\chi} r(w\sin\psi - u\cos\psi)) \tag{D.4}$$

$$M^{ST} = (Q_{\xi\xi} q(w\sin\theta - u\cos\theta) + Q_{\xi\chi} r(w\sin\psi - u\cos\psi)) \tag{D.5}$$

$$N^{ST} = (Q_{\chi\xi} q(w\sin\theta - u\cos\theta) + Q_{\chi\chi} r(w\sin\psi - u\cos\psi)) \tag{D.6}$$

Appendix E. Hydrostatic restoring forces and moments

Hydrostatic restoring coefficients are found using the following equations.

$$Z_z = \rho g \int_L \left(\frac{c_1}{2} + \frac{c_2}{2} \right) dx \tag{E.1}$$

$$Z_\varphi = -\rho g \int_L \left(\frac{c_1^2}{2} - \frac{c_2^2}{2} \right) dx \tag{E.2}$$

$$Z_\theta = -\rho g \int_L \left(\frac{c_1}{2} + \frac{c_2}{2} \right) x dx \tag{E.3}$$

$$K_z = \rho g \int_L \left(\frac{c_1^2}{6} - \frac{c_2^2}{6}\right) dx \tag{E.4}$$

$$K_\varphi = \rho g \int_L \left(\frac{c_1^3}{6} + \frac{c_2^3}{6}\right) dx \tag{E.5}$$

$$K_\theta = -\rho g \int_L \left(\frac{c_1^2}{6} - \frac{c_2^2}{6}\right) x dx \tag{E.6}$$

$$M_z = \rho g \int_L \left(\frac{c_1}{2} + \frac{c_2}{2}\right) x dx \tag{E.7}$$

$$M_\varphi = -\rho g \int_L \left(\frac{c_1^2}{2} - \frac{c_2^2}{2}\right) x dx \tag{E.8}$$

$$M_\theta = -\rho g \int_L \left(\frac{c_1}{2} + \frac{c_2}{2}\right) x^2 dx \tag{E.9}$$

References

Bhawsinka, K., 2008. Maneuvering Simulation of Displacement Type Ships and Planing Hull. M.Sc thesis. Memorial University of Newfoundland, Newfoundland, Canada.

Blount, D.L., Codega, L.T., 1992. Dynamic stability of planing crafts. Mar. Technol. 29, 4–12.

Bowles, J., Blount, D.L., 2012. Turning characteristics and capabilities of high-speed monohulls. In: Paper Presented at: Proceedings of the Third Chesapeake Powerboat Symposium. Annapolis, MD.

Brown, P.W., Klosinski, W.E., 1994. Directional Stability Tests of Two Prismatic Planing Hull. Stevens institute of technology, US Coast Guard, Hoboken, New Jersey.

Brown, P.W., Klosinski, W.E., 1994. Directional Stability Tests of a 30 Degrees Deadrise Prismatic Planing Hull. Stevens Institute of Technology, US Coast Guard, Hoboken, New Jersey.

Dashtimanesh, A., Tavakoli, S., Sahoo, P.K., 2017. A simplified method to calculate trim and resistance of a two-stepped planing hull. Ships Offshore Struct. 12 (Suppl. 1), S317–S329.

Dashtimanesh, A., Enshaeei, H., Tavakoli, S., 2019. Oblique-asymmetric 2D+ T model to compute hydrodynamic forces and moments in coupled sway, roll, and yaw motions of planing hulls. J. Ship Res. 63 (1), 1–15.

Dashtimanesh, A., Roshan, F., Tavakoli, S., Kohansal, A., Barmala, F., 2019. Effects of step configuration on hydrodynamic performance of one-and doubled-stepped planing flat plates: a numerical simulation. P I Mech Eng M-J Eng Maritime Environment. https://doi.org/10.5957/JSPD.11170053 (in press).

Denny, S.B., Hubble, E.N., 1991. Prediction of craft turning characteristics. Mar. Technol. 28 (1), 13.

Esfandiari, A., Tavakoli, S., Dashtimanesh, A., 2019. Comparison between the Dynamic behavior of the non-stepped and double-stepped planing hulls in rough water: a numerical study. Proc. Inst. Mech. Eng. M J. Eng. Marit. Environ. https://doi.org/10.1177/1475090219851917 (in press).

Faltinsen, O.M., Kjaerland, O., Nøttveit, A., Vinje, T., 1977. Water Impact Loads and Dynamic Response of Horizontal Circular Cylinders in Offshore Structures. Offshore Technology Conference.

Garme, K., 2005. Improved time domain simulation of planing hulls in waves by correction of near-transom lift. Int. Shipbuild. Prog. 52, 201–230.

Garme, K., Rosen, A., 2003. Time domain simulations and full-scale trials on planing crafts in waves. Int. Shipbuild. Prog. 50 (3), 177–208.

Ghadimi, P., Tavakoli, S., Dashtimanesh, A., Pirooz, A., 2014. Developing a computer program for detailed study of planing hull's spray based on Morabito's approach. J. Mar. Sci. Appl. 13, 402–415.

Ghadimi, P., Tavakoli, S., Feizi Chekab, M.A., Dashtimanesh, A., 2015. Introducing a particular mathematical model for predicting the resistance and performance of prismatic planing hulls in calm water by means of total pressure distribution. J. Nav. Archit. Mar. Eng. 12, 73–94.

Ghadimi, P., Tavakoli, S., Dashtimanesh, A., 2016. An analytical procedure for time domain simulation of roll motion of the warped planing hulls. P I Mech Eng M-J Eng, Maritime Environment 230, 600–615.

Ghadimi, P., Tavakoli, S., Dashtimanesh, A., 2016. Coupled heave and pitch motions of planing hulls at non-zero heel angle. Appl. Ocean Res. 59, 286–303.

Ghadimi, P., Tavakoli, S., Dashtimanesh, A., 2016. Calm water performance of hard-chine vessels in semi-planing and planing regimes. Pol. Marit. Res. 4, 23–45.

Ghadimi, P., Tavakoli, S., Dashtimanesh, A., Zamanian, R., 2017. An analytical procedure for time domain simulation of roll motion of the warped planing hulls. P I Mech Eng M-J Eng Maritime Environment 230, 600–615.

Ghadimi, P., Tavakoli, S., Dashtimanesh, A., Zamanian, R., 2017. Steady performance prediction of a heeled planing craft in calm water using asymmetric 2D+T model. P I Mech Eng M-J Eng Maritime Environment 231, 234–257.

Ghadimi, P., Tavakoli, S., Dashtimanesh, A., Taghikhani, P., 2017. Dynamic response of a wedge through asymmetric free fall in 2 degrees of freedom. P I Mech Eng M-J Eng Maritime Environment. https://doi.org/10.1177/1475090217733150. Published Online.

Ghadimi, P., Panahi, S., Tavakoli, S., 2019. Hydrodynamic study of a double-stepped planing craft through numerical simulations. J. Braz. Soc. Mech. Sci. Eng. 41, 1–15.

Izadi, M., Ghadimi, P., Fadavi, M., Tavakoli, S., 2018. Hydroelastic analysis of water impact of flexible asymmetric wedge with an oblique speed. Meccanica 53 (10), 2585–2617.

Javanmardi, N., Ghadimi, P., Tavakoli, S., 2018. Probing into the effects of cavitation on hydrodynamic characteristics of surface piercing propellers through numerical modeling of oblique water entry of a thin wedge. Brodogradnja: Teorija i praksa brodogradnje i pomorske tehnike 69 (1), 151–168.

Judge, C., Troesch, A., Prelin, M., 2004. Initial water impact of a wedge at vertical and oblique angles. J. Eng. Math. 48, 279–303.

Katayama, T., Kimoto, R., Iida, T., Ikeda, Y., 2005. Effects of running attitudes on hydrodynamic forces for oblique towed planing craft. J Kansai Society of Naval Architecture 243, 15–22.

Katayama, T., Iida, T., Ikeda, Y., 2006. Effects of change in running attitude on turning diameter of planing craft. In: Paper Presented at: Proceedings of the 2nd PAMES and AMEC 2006, Jeju, Korea.

Katayama, T., Taniguchi, T., Fuji, H., Ikeda, Y., 2009. Development of maneuvering simulation method for high speed craft using hydrodynamic forces obtained from model tests. In: Paper Presented at: 10th International Conference on Fast Sea Transportation (FAST 2009), Athens, Greece.

Kim, D.J., Kim, S.Y., 2017. Turning characteristics of waterjet propelled planing craft at semi-planing speeds. Ocean. Eng. 143, 24–33.

Korobkin, A.A., Malenica, 2005. Modified Logvinovich Model for Hydrodynamic Loads on Asymmetric Contours Entering Water. 20th International Workshop on Water Waves and floating Bodies, Oslo.

Lewandowski, E.M., 1994. Trajectory prediction for high-speed planing craft. Int. Shipbuild. Prog. 41, 137–148.

Lewandowski, E.M., 1995. The transverse dynamic stability of hard chine planing craft. In: Paper Presented at: Proceedings of the Sixth International Symposium on Practical Design of Ships and Mobile Units, Seoul, Korea.

Matrin, M., 1976. Theoretical Prediction of Motions of High-Speed Planing Boats in Waves. DTNSRDC, Bethesda, MD, USA. Report 76-0069.

Morabito, M.G., 2014. Empirical equations of planing hull bottom pressures. J. Ship Res. 58, 185–200.

Morabito, M.G., 2015. Prediction of planing hull side forces in yaw using slender body oblique impact theory. Ocean. Eng. 101, 45–57.

Morabito, M., Pavkov, M., Timmins, Beaver B., 2014. Experiments on directional stability of stepped planing hulls. In: Paper Presented at: the 4th Chesapeake Power Boat Symposium, Annapolis, MD, US.

Newman, N., 1977. Marine Hydrodynamics. MIT Press.

Niazmand Bilandi, R., Dashtimanesh, A., Tavakoli, S., 2019. Development of a 2D+ T theory for performance prediction of double-stepped planing hulls in calm water. P I Mech Eng M-J Eng Maritime Environment 233 (3), 886–904.

Payne, P.R., 1988. Design of High Speed Boats, ume 1. Planing, Fishergate Inc, Annapolis, Maryland.

Payne, P.R., 1995. Contributions to planing theory. Ocean. Eng. 22, 699–729.

Qin, H., Zhao, L., Shen, J., 2011. A Modified Logvinovich model for hydrodynamic loads on an asymmetric wedge entering water with a roll motion. J. Mar. Sci. Appl. 10, 184–189.
Savitsky, D., 1964. Hydrodynamic design of planing hulls. Mar. Technol. 1, 71–95.
Savitsky, D., Prowse, R.E., Lueders, D.H., 1958. High-speed Hydrodynamic Characteristics of a Flat Plate and 20° Dead-Rise Surface in Unsymmetrical Planing Condition. NACA Technical Note, 4187.
Smiley, R.F., 1952. A Theoretical and Experimental Investigation of the Effects of Yaw on Pressure, Forces and Moments during Seaplane Landings and Planing. NACA Technical Note. No 2817.
Submaranian, R., Beck, R., 2015. A time-domain strip theory approach to maneuvering in a seaway. Ocean. Eng. 104, 107–118.
Sugai, K., 1964. On the Maneuverability of the High-Speed Craft. Transportation Technical Research Institute, Ministry of Transportation, 1-1057, Meijiro-Cho, Toshinas-Ku, Tokyo, 12(11).
Sun, H., Faltinsen, O.M., 2007. Hydrodynamic forces on a planing hull in forced heave or pitch motions in calm water. In: Paper Presented at: Proceedings of the 22nd International Workshop on Water Waves and Floating Bodies, Plitvice, Croatia.
Tajima, S., Ikeda, Y., Katayama, T., Okumura, H., 1999. Measurements of hydrodynamic forces acting on planing hull at high-speed by planar motion mechanism test. J. Kansai Soc. Naval Archit. 232, 71–76.
Tavakoli, S., Dashtimanesh, A., 2017. Running attitudes of yawed planing hulls in calm water: development of an oblique 2D+T approach. J. Ship. Offshore. Struct. 12 (8), 1086–1099.
Tavakoli, S., Dashtimanesh, A., 2018. Mathematical simulation of planar motion mechanism test for planing hulls by using 2D+ T theory. Ocean. Eng. 169, 651–672.
Tavakoli, S., Ghadimi, P., Dashtimanesh, A., Sahoo, P.K., 2015. Determination of hydrodynamic coefficients related to roll motion of high-speed planing hulls. In: Proceedings of the 13th Fast Sea Transportation (FAST 2015), DC, US.
Tavakoli, S., Dashtimanesh, A., Mancini, S., 2018. A theoretical method to explore the influence of free roll motion on the behavior of a high-speed planing vessel through a steady yawed motion. Int. J. Small Craft technol. 160 (B2), B67–B77. Jul-Dec 2018.
Tavakoli, S., Dashtimanesh, A., Sahoo, P.K., 2017. An oblique 2D+T approach for hydrodynamic modeling of yawed planing crafts in calm water. J. Ship. Prod. Design. Pub. Online. https://doi.org/10.5957/JSPD.160032.
Tavakoli, S., Ghadimi, P., Dashtimanesh, A., 2017. A nonlinear mathematical model for coupled heave, pitch, and roll motions of a high-speed planing hull. J. Eng. Math. 104, 157–194.
Tavakoli, S., Dashtimanesh, A., Sahoo, P., 2018. Prediction of hydrodynamic coefficients of coupled heave and pitch motions of heeled planing boats by asymmetric 2D+T theory. In: ASME 2018 37th International Conference on Ocean. Offshore and Arctic Engineering, Madrid, Spain.
Tavakoli, S., Najafi, S., Amini, E., Dashtimanesh, A., 2018. Performance of high-speed planing hulls accelerating from rest under the action of a surface piercing propeller and an outboard engine. Appl. Ocean Res. 77, 45–60.
Toxopeus, S., 1996. A Time Domain Simulation Program for Maneuvering of Planing Ships. Delft University of Technology, Faculty of Mechanical Engineering and Marine Technology, Delft, Netherland.
Toxopeus, S., 1996. Mathematical Model of the Behaviour of Planing Ships. Delft University of Technology, Faculty of Mechanical Engineering and Marine Technology, Delft, Netherland.
von Karman, T., 1929. The Impact of Seaplanes Floats during Landing. National Advisory Committee for Aeronautics, Washington DC.
Xu, L., Troesch, A.W., Peterson, R., 1999. Asymmetric hydrodynamic impact and dynamic response of vessels. J. Offshore Mech. Arct. Eng. 121, 83–89.
Zarnick, E.E., 1978. A n. In: Onlinear Mathematical Model of Motions of a Planing Boat in Regular Waves. Bethesda, MD, USA.